Int. J. of Applied Mechanics and Engineering, 2017, vol.22, No.4, pp.995-1017
DOI: 10.1515/ijame-2017-0064

COUPLED FINITE VOLUME AND FINITE ELEMENT METHOD ANALYSIS OF A COMPLEX LARGE-SPAN ROOF STRUCTURE

J. SZAFRAN, K. JUSZCZYK and M. KAMIŃSKI*
Department of Structural Mechanics
Faculty of Civil Engineering, Architecture and Environmental Engineering
Technical University of Łódź
Al. Politechniki 6, 90-924 Łódź, POLAND
E-mails: Jacek.Szafran@p.lodz.pl
klaudiaa.juszczyk@gmail.com
Marcin.Kaminski@p.lodz.pl

The main goal of this paper is to present coupled Computational Fluid Dynamics and structural analysis for the precise determination of wind impact on internal forces and deformations of structural elements of a long-span roof structure. The Finite Volume Method (FVM) serves for a solution of the fluid flow problem to model the air flow around the structure, whose results are applied in turn as the boundary tractions in the Finite Element Method problem structural solution for the linear elastostatics with small deformations. The first part is carried out with the use of ANSYS 15.0 computer system, whereas the FEM system Robot supports stress analysis in particular roof members. A comparison of the wind pressure distribution throughout the roof surface shows some differences with respect to that available in the engineering designing codes like *Eurocode*, which deserves separate further numerical studies. Coupling of these two separate numerical techniques appears to be promising in view of future computational models of stochastic nature in large scale structural systems due to the stochastic perturbation method.

Key words: CFD simulation, Finite Volume Method, Finite Element Method, wind engineering.

1. Introduction

Wind engineering has been under active development since many years due to multiple reasons ranging from treating wind energy as a renewable energy source, through utilizing wind to improve life conditions and increasing security measures against wind impact on people and the environment ([1], [2]), up to measuring its effective impact on engineering structures and buildings ([3], [4], [5]).

Wind, as an atmospheric phenomenon, treated as a large-scale (macroscopic) air flow characterized by formation of vortexes and other coherent structures, is defined in fluid mechanics as a turbulent flow. Turbulence is arguably the most challenging area in fluid dynamics and the most limiting factor in accurate computer simulation of engineering flows. It constitutes a classical multi-scale problem, which is far beyond human intuitive understanding and also beyond resolution capabilities of even the most powerful modern parallel computers ([6]). Various analyses of the wind impact, character, incidence, and variability over time have been made for years. Aerodynamic wind tunnel tests, although still developed and used, were getting replaced by computer analyses with fluid mechanics assumptions ([7], [8]).

The wind load is one of the fundamental types of interactions in civil engineering problems, particularly in slender light structures like towers, chimneys, masts, and maybe the most important - open and/or semi-open structural large-span roofs ([9]). Computational Fluid Dynamics (CFD) analyses allow simulation of the turbulent flow around a solid non-deformable object and computations of various state parameters, such as velocity profiles discrete values, pressure, temperature, streamlines or pressure

* To whom correspondence should be addressed

coefficients which, depending on its character, can be observed either around or on the surface of the analyzed body. CFD techniques, in the context of interactions in-between the wind loading and stress distributions, particularly in structural elements, are presented and developed in a variety of research works. The very challenging problem would be a full iterative fluid-solid interaction in-between the PVT (pressure-temperature-velocity) solution made during CFD and large deformations of the structure, where the nonlinear deformation process in structural elements (i.e. during fire) significantly affects the external boundaries inserted into the CFD domain, etc.

Vizotto and Ferreira [10] presented the wind pressure coefficient for a non-conventional building of the free form shell structure generated by the simulation of a membrane initially in the horizontal plane surface with hexagonal plant, under the dead load and supported on six corners. They perform a numerical analysis on a scale model of a free form shell structure by the computational fluid dynamics software and compare the results against the wind force coefficients obtained by the wind tunnel tests. These studies prove that there is a similarity between the results of the mean force coefficients obtained by the computational model and these obtained experimentally in the wind tunnel test. It can be therefore concluded that air flow analyses in CFD software allow the verification of the behavior of these structures under wind action. An advantage of computer load is that it does not have the physical limitation of the scale model in the wind tunnel. In [11] the authors conducted research on predicting wind loads on and wind flow around tall steel building. They performed analyses concerning wind effects on buildings using CFD techniques. The computed results were compared with the extended experimental data obtained in seven wind tunnel tests, which revealed some discrepancies: it was found that the velocity profile of the approaching wind flow influences, mainly the mean pressure coefficients for the building and the incident turbulence intensity profile, had a significant effect on the fluctuating wind forces. Predicting wind-influence vibrations on high-rise buildings using unsteady CFD and modal analysis is the subject of [12]. The authors concluded that a numerical procedure using unsteady CFD methodologies and the modal analysis are a practical tool to assess wind induced vibrations of tall buildings in early stages of design. The numerical accuracy is satisfactory and the computational costs are much less than for the Fluid Structure Interaction analyses.

The impact the wind has on human comfort, urban development design, and town and country planning are undeniably areas of application for CFD analyses. The issue was discussed in [13], [14] and [15] – the authors of [13] and [14] engaged in sports stadium analyses in terms of protection against wind-driven rain in different types of stadium geometry and its effect on wetting the stands, which is the crucial aspect of spectator comfort, and pedestrian wind comfort around a stadium in an urban environment. Three - dimensional steady-state Reynolds-averaged Navier-Stokes (RANS) Computational Fluid Dynamics simulations of wind flow are utilized in both cases. Authors of [15] used CFD to obtain detailed aerodynamic information about wind flow in urban area. They analyzed pedestrian wind comfort and wind safety at the campus of Eindhoven University of Technology. The turbulent wind flow patterns over the campus terrain have been obtained by solving the 3D steady Reynolds-averaged Navier-Stokes equations with the realizable k-ε model on an extensive high-resolution grid based on grid-convergence analysis.

The wind phenomenon is expected to be used as the renewable energy source and the CFD simulations are used to design wind turbines by wind power experts. Research results in this area can be found in [16] and [17]. The next area of application for Computational Fluid Dynamics simulations is green building, where the above mentioned research results are used to improve the existing solutions and to develop the new ones, e.g., effective natural ventilation system. Authors of [6] ran two-dimensional and three-dimensional simulations of the ventilation performance using CFD and compared the results with earlier wind tunnel experiments. They ascertained that the simulation results support the wind tunnel experiment and CFD is a useful numerical tool for the study of fluid flow.

Nowadays, the designed structures have sophisticated, unconventional shapes that require an individual approach beyond standard design guidelines, including wind load standards. CFD analyses make it possible to tackle the issues concerning wind impact by determination of parameters for air flow around and on the surface of objects, e.g., velocity distribution or pressure coefficients. This topic was discussed in [18] and [19].

The civil engineering structure under consideration in this study is Hannover Messe/Laatzen station building. The building has been erected on a rectangular base and it has one of its sidewalls designed with the angle of about 82 degrees with respect to the ground level. It resembles a single surface ended with a sector of a circle, which bases itself on the edges of these sidewalls. An essential part of the structure is the roof: a three layer spatial lattice, which forms an unusually complex geometric layout. The CFD analysis was carried out to find out the wind flow around the building and the impact the wind has on its surface, and what is more important from the structural point of view, on cross-sectional forces of the roof structural members. It is mandatory to mention that interfacing in-between FVM and FEM analyses is not straightforward – the grid and the mesh relevant to each of these methods have different density and different location of the nodal points. Therefore, the pressures resulting from the CFD analysis are inserted further into the FEM model as the surface boundary tractions that are distributed automatically by the ROBOT system into the additional nodes in the mesh [20].

2. Mathematical model

2.1. CFD analysis

The starting point for Reynolds equations are momentum conservation principles called Navier-Stokes equations. It is obviously known that analytical solutions to the Navier-Stokes equation system for the turbulent flow [20] are very rare and they can be obtained for really very simple fluid flow cases. The equations with excluded transient heat transfer and temperature dependence of all physical paramters are introduced traditionally as

$$f_i - \frac{1}{\rho}\frac{\partial p}{\partial x_i} + \frac{\mu}{\rho}\frac{\partial^2 v_i}{\partial x_j^2} + \frac{1}{3}\cdot\frac{\mu}{\rho}\cdot\frac{\partial}{\partial x_i}\frac{\partial v_j}{\partial x_j} = \frac{dv_i}{dt} + v_j\frac{\partial v_i}{\partial x_j} \tag{2.1}$$

where i, j denote Cartesian coordinates relevant to the three dimensional flow, and f_i is the vector of body forces, p is the static pressure, v_i denotes the velocity vector component, ρ is density of the medium, t is time, μ the is dynamic viscosity coefficient. Various terms of Navier-Stokes equations represent, in turn, unit forces (per a unit of the mass): force adjacent to active mass force, normal surface force, tangential surface force caused by the fluid viscosity, tangential surface force caused by the fluid compressibility, and passive mass force (inertia force). Usually, the Navier-Stokes equation system for an incompressible fluid is described as

$$f_i - \frac{1}{\rho}\frac{\partial p}{\partial x_i} + \frac{\mu}{\rho}\frac{\partial^2 v_i}{\partial x_j^2} = \frac{dv_i}{dt} + v_j\frac{\partial v_i}{\partial x_j}. \tag{2.2}$$

In order to obtain the solution to the partial equations above, variation formulas are used, where equations are numerically integrated within a given finite volume. This operation gives us the balance equations in the following form

$$\int_\Omega \delta v_i \rho\left(\dot{v}_i + \frac{\partial v_i}{\partial x_j}v_j\right)d\Omega + \int_\Omega d\frac{\partial v_i}{\partial x_j}\left(2\mu\varepsilon_{ij} - p\delta_{ij}\right)d\Omega = \int_\Omega \delta v_i \tilde{f}_i d\Omega + \int_{\partial\Omega} \delta v_i \tilde{f}_i d\left(\partial\Omega_\sigma\right), \tag{2.3}$$

$$\int_\Omega \delta p\frac{\partial v_i}{\partial x_i}d\Omega = 0 \tag{2.4}$$

where δ_{ij} is the Kronecker delta and ε_{ij} is a small strain tensor traditionally defined as

$$\varepsilon_{ij} = \frac{1}{2}\left(\frac{\partial v_i}{\partial x_j} + \frac{\partial v_j}{\partial x_i} \right). \tag{2.5}$$

If we substitute temporary flow parameters with average values (averaged over time, called Reynolds-averaged Navier–Stokes equations or RANS equations), we obtain averaged turbulent flow equations (Reynolds equations) in which additional turbulent stresses (Reynolds stress) occur (8) induced by momentum transfer in fluctuation movement. Hence, the Reynolds equations system yields

$$\frac{\partial v_i}{\partial t} + \overline{v}_j \frac{\partial \overline{v_i}}{\partial x_j} = \overline{f_i} - \frac{1}{\rho}\frac{\partial \overline{p}}{\partial x_i} + \nu \nabla^2 \overline{v_i} + \frac{1}{\rho}\frac{\partial}{\partial x_j}\left(-\rho \overline{v_i' v_j'} \right), \tag{2.6}$$

where $\overline{f_i}$ is the average value of external forces vector component (unit mass forces), $\overline{p}$ is the average value of static pressure, $\overline{v_i}$ is the average value of velocity vector component, $\nu = \frac{\mu}{\rho}$ means the kinematic viscosity coefficient and $\nabla^2 \equiv \frac{\partial^2}{\partial x^2} + \frac{\partial^2}{\partial y^2} + \frac{\partial^2}{\partial z^2}$ is the Laplace operator. Further, continuity equations system for incompressible fluid ($\rho = \text{const}$) is given as

$$\frac{\partial \overline{v_j}}{\partial x_j} = 0 \tag{2.7}$$

and turbulent stresses are equal to

$$\overline{\tau_{ij}} = -\rho \overline{v_i' v_j'}\,. \tag{2.8}$$

Reynolds equations yield mass and momentum conservation principle in averaged turbulent flow, which is very convenient for further application of the Finite Volume Method. Numerical simulation of turbulent air flow in near-surface area of an object, which is presented in this work, has been conducted by using the *k*-ε model. It describes the relationship in-between the turbulence kinetic wind energy *k* (turbulence energy) and the turbulence dissipation coefficient ε (energy dissipation). The following equation of the turbulence kinetic energy *k* is applied

$$\frac{\partial}{\partial t}(\rho k) + \frac{\partial}{\partial x_j}\left(\rho k v_j\right) = \frac{\partial}{\partial x_j}\left[\left(\mu + \frac{\mu_t}{\sigma_k} \right) \frac{\partial k}{\partial x_j} \right] + G_k - \rho\varepsilon\,, \tag{2.9}$$

while the equation of turbulence kinetic energy dissipation is rewritten as

$$\frac{\partial}{\partial t}(\rho\varepsilon) + \frac{\partial}{\partial x_j}\left(\rho \varepsilon v_j\right) = \frac{\partial}{\partial x_j}\left[\left(\mu + \frac{\mu_t}{\sigma_\varepsilon} \right) \frac{\partial \varepsilon}{\partial x_j} \right] + \rho C_{\varepsilon 1} s_\varepsilon - \rho C_{\varepsilon 2} \frac{\varepsilon^2}{k + \sqrt{\nu\varepsilon}} \tag{2.10}$$

where μ_t is the turbulent dynamic viscosity. The specific equations describing parameters in this model are given as follows

$$C_{\varepsilon 1} = \max\left[0.43;\ \frac{\eta}{\eta+5}\right],$$

$$\eta = s\frac{k}{\varepsilon},$$

$$s = \sqrt{2s_{ij}s_{ij}}, \tag{2.11}$$

$$s_{ij} = \frac{1}{2}\left(\frac{\partial v_i}{\partial x_j} + \frac{\partial v_j}{\partial x_i}\right),$$

$$G_k = -\rho\overline{v_i' v_j'}\frac{\partial v_j}{\partial x_i},$$

$$\mu_t = \rho \cdot C_\mu \frac{k^2}{\varepsilon} \quad .$$

The realizable k-ε model differs from the standard k-ε model in the sense that the value of C_μ is not constant, but a variable influenced by average flow (average distortion) and turbulence (k – ε). The quantities $C_{\varepsilon 2}$, σ_k and σ_ε have been adopted as $C_{\varepsilon 2} = 1{,}9$, $\sigma_k = 1{,}0$ and $\sigma_\varepsilon = 1{,}2$, correspondingly.

Therefore, the wind flow problem analysis is reduced to a solution of the differential equations system, which contains (a) continuity equations, (b) Reynolds equations, and (c) the realizable k-ε model equations. As a result, the following flow parameters are obtained (a) pressure, (b) velocity vector components, (c) kinetic energy of turbulence, (d) dissipation of kinetic energy of turbulence, (e) turbulent dynamic viscosity of a fluid ([21]).

The wind is assumed to be incompressible, so that the solution method is based upon the pressure-based segregated algorithm. The steady-state analysis type and SIMPLE algorithm have been used as the flow solver to guarantee the first order accuracy. The computer algorithm solves here momentum equations and obtains the velocity vector field, which may not satisfy the mass equation. Then, this algorithm performs velocity and pressure corrections in order to satisfy the continuity equation. This correction is repeated until a given precision of solution is achieved. The individual governing equations for the solution variables are solved one after another in the segregated algorithm.

2.2. Structural problem

After successful solution of the Reynolds equations we use the pressures as the stress boundary conditions for further Finite Element Method analysis of the structural linear elastic problem. Let us consider for this purpose the region Ω. Let us assume that there are non-empty subsets of external boundaries of Ω, namely $\partial\Omega_\sigma$ and $\partial\Omega_u$, where the stress (following the CFD problem solution) and displacement boundary conditions are defined. The equilibrium equations system can be written as follows

$$\sigma_{ij} = C_{ijkl}\varepsilon_{kl}\,, \tag{2.12}$$

$$\varepsilon_{ij} = \frac{1}{2}\left(\frac{\partial u_i}{\partial x_j} + \frac{\partial u_j}{\partial x_i}\right), \tag{2.13}$$

$$\sigma_{ij,j} + \rho f_i = 0\ , \tag{2.14}$$

$$u_i = \hat{u}_i\,; \qquad x_i \in \partial\Omega_u\,, \tag{2.15}$$

$$\sigma_{ij}\ n_j = \hat{t}_i\,; \qquad x_i \in \partial\Omega_\sigma\,, \tag{2.16}$$

where

$$C_{ijkl} = \delta_{ij}\delta_{kl}\frac{e\nu}{(1+\nu)(1-2\nu)} + \left(\delta_{ik}\delta_{jl} + \delta_{il}\delta_{jk}\right)\frac{e}{2(1+\nu)}, \tag{2.17}$$

for *i*, *j*, *k*, *l=1*, *2*, *3*. Generally, this system of equations is frequently solved using the following variational formulation known as the virtual work principle

$$\int_\Omega C_{\alpha\beta\gamma\delta}u_{\alpha,\beta}\delta u_{\gamma,\delta}\,d\Omega = \int_\Omega \rho f_\alpha \delta u_\alpha\,d\Omega + \int_{\partial\Omega_\sigma} \tilde{t}_\alpha \delta u_\alpha\,d(\partial\Omega) \tag{2.18}$$

where the left hand side of Eq.(2.18) corresponds to elastic behavior of the structure, the first component on the right side includes the body forces effects, while the last one is equivalent to the stress boundary conditions applied.

3. Computational implementation

3.1. CFD analysis

The basic idea behind the Finite Volume Method (FVM) ([22], [23], [24]) is an application of the Ostrogradski-Gauss divergence theorem to replace the volumetric integrals inherent to the governing equation with the surface integrals rewritten for all the finite volumes completely composing the entire computational domain. A contribution of each finite volume to the global equilibrium equation is represented here as the contribution of its center as well as its outer faces, which differs from the Finite Element Method discretization, where a contribution of each element traditionally results from its nodal points contributions. Then, the Reynolds equation is discretized in each finite volume *l* as

$$\begin{aligned}&\left(\frac{\rho^{(\alpha)}\Delta U^{(\alpha)}}{\Delta t}\right)_l + \frac{1}{V_l}\sum_{j=1}^{n_s}\rho_j{}^{(\alpha)}U_j{}^{(\alpha)}A_j - \frac{1}{V_l}\sum_{j=1}^{n_s}\mu_j{}^{(\alpha)}\nabla U_j{}^{(\alpha)}A_j = \\ &= \left(\nabla U^{(\alpha)}\right)_l \nabla\mu_l{}^{(\alpha)} - \left(\nabla P^{(\alpha)}\right)_l + \rho_l{}^{(\alpha)}g^{(\alpha)}\end{aligned} \tag{3.1}$$

where V_l is the *l* th finite volume, ρ is the fluid density, Δt is time increment, μ is the fluid viscosity, g is gravitational acceleration. The pressure gradient in the x_i direction is calculated here using the Gauss integration scheme as

$$\nabla P_l^{(\alpha)}(x_i) = \frac{1}{V_l}\sum_{j=1}^{n_s} P_j^{(\alpha)} A_j n_j , \tag{3.2}$$

where A_j is the area of the j face, n_j is the versor of this surface directed outwards, $\alpha = 1,..,M-M$ denotes the total number of computational iterations. We obtain analogously for the velocities

$$\nabla U_l^{(\alpha)} = \frac{1}{V_l}\sum_{j=1}^{n_s} U_j^{(\alpha)} A_j n_j \tag{3.3}$$

where the central differencing scheme is applied to determine the averaged value at the cell face center.

3.2. Structural problem

Let us introduce the following approximation for the displacement field using classical shape functions $\phi_{i\alpha}(x)$

$$u_i(x) = \varphi_{i\alpha}(x)\, q_\alpha , \qquad x_i \in \Omega , \tag{3.4}$$

$i = 1,2$; $\alpha = 1,...,N$ (N is the total number of degrees of freedom introduced in Ω) and $k=1,\ldots,n$. The strain tensor components are discretized analogously. The following representation of the strain tensor components is obtained

$$\varepsilon_{ij}(x) = B_{ij\alpha}(x)\cdot q_\alpha , \qquad x_i \in \Omega , \tag{3.5}$$

where $B_{ij\alpha}(x_k)$ is the matrix of the shape functions derivatives

$$B_{ij\alpha}(x) = \tfrac{1}{2}\left[\phi_{i\alpha,j}(x_k) + \phi_{j\alpha,i}(x_k)\right], \qquad x_i \in \Omega . \tag{3.6}$$

The FEM approach in the context of the above discretization is equivalent to the linear algebraic equations system

$$K_{\alpha\beta} q_\beta = Q_\alpha \tag{3.7}$$

where q_β is the resulting displacements vector, $K_{\alpha\beta}$ denotes the stiffness matrix, and Q_α stands for the external forces vector. Let us recall the classical definition of the stiffness matrix in the form of

$$K_{\alpha\beta} = \sum_{e=1}^{E} \int_{\Omega_e} C_{ijkl}^{(e)} B_{ij\alpha} B_{kl\beta}\, d\Omega \tag{3.8}$$

where $C_{ijkl}^{(e)}$ stands for the elasticity tensor components inside the finite element 'e' and E is their total number within Ω.

4. Large-span roof structure analysis

The FEM computer system ANSYS 15.0 CFD has been used for a solution to the fluid mechanics problem and this is done by using the FVM ([25], [26], [27], [28]). It treats the wind flow as a turbulent motion of a homogeneous, incompressible, viscous fluid ($\rho = \text{const}$, $\mu = \text{const}$) and is uniquely described by the Reynolds equations and the continuity equation. The roof cover of the analyzed steel structure may be treated as the light-weight construction having complex structure with a large span of bearing elements: *40.0 m* (Fig.1). Its static system is presented in Figs 1-3.

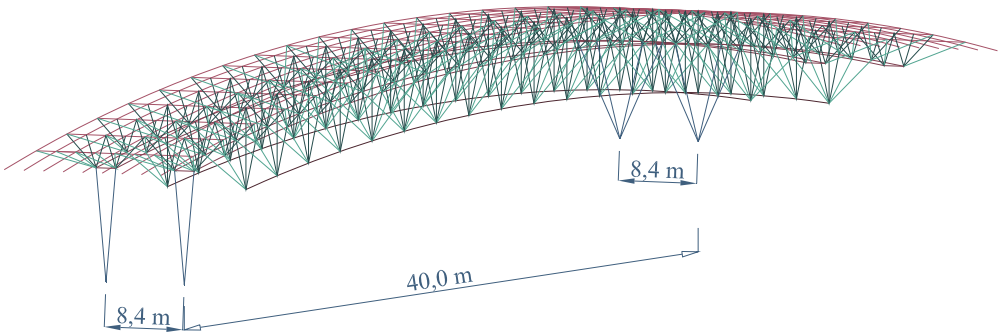

Fig.1. Axonometric view of the analyzed roof structure.

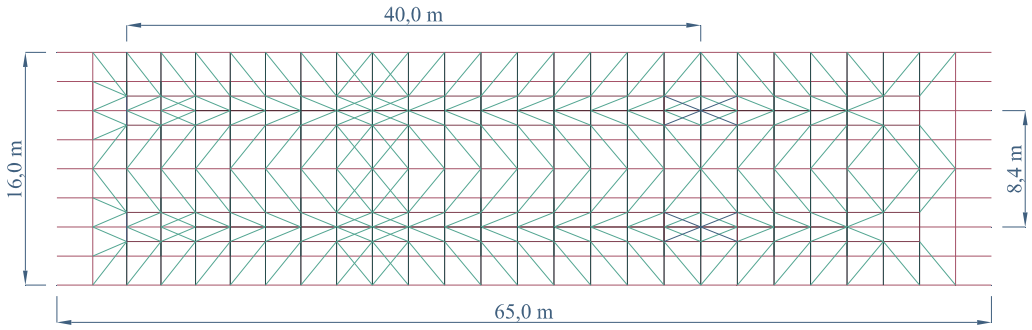

Fig.2. Top view of the long-span roof.

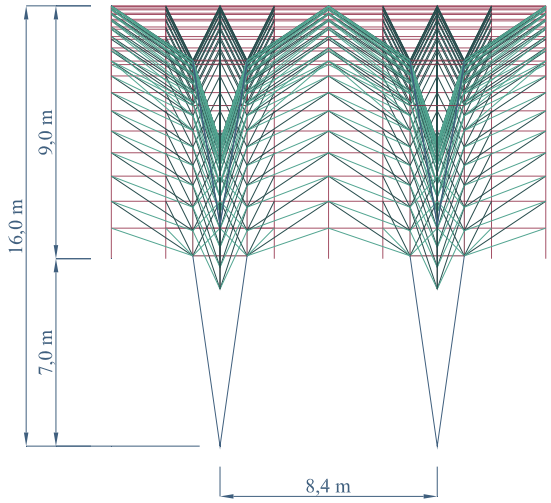

Fig.3. Structural system of the analyzed roof.

Spatial distribution of the structural elements shown above results in many difficulties, even in the initial design phase, when the possibility of realization has to be determined and uniquely determined specific optimal element profiles have to be adopted with their geometrical and material parameters. In order to correctly estimate the internal forces distribution in given elements, which is not trivial due to the multilayer and multidirectional beam configuration of the cover structure, the influence on the roof surface must be determined in a very accurate way. There is no doubt that the wind action is the main factor that determined the geometrical parameters for the designed layout for these types of structural covers. The available design standard [29] offers only some roughly approximated estimates for the wind load by using huge simplifications, which can be insufficient for such specific large scale structures; Therefore, the principal goal of this analysis is a precise determination of the wind impact, which in turn would allow an accurate estimation of internal forces in the beams forming the complex multilayer roof cover structure. In order to do that, the CFD problem has been solved by modeling the air flow around the analyzed object and by observing (through the external pressure coefficients) its action on this structure. The roof structure was erected on a base of *60 x 16 m* rectangle, three of its walls were vertical and one of the gabble walls was sloped in relation to the ground level at the angle of 82 degrees in such a way that it formed an obtuse angle with the other wall. Other geometrical dimensions are shown in Fig.4.

A compact building body has been inserted into a computational domain, where a wind simulation has been carried out and for this purpose Gambit 2.4.6 computer program (an integrated preprocessor for CFD programs) was used. The dimensions of the body were defined based on the guidelines from [30], though some modifications were applied. Initially, the rules for proper modeling of space around an analyzed object have been adopted to ensure that the analysis of impact on a three-dimensional object and surrounding terrain is correct. In the analyzed case, no aerodynamic analysis of wind flow around the structure has been carried out, because its action on the surrounding terrain was insignificant contrary to its action on the building surface. Therefore, it was decided to reduce the size of the domain in order to reduce the number of finite volumes and to shorten considerably the overall time of these computations; the adopted domain dimensions are shown in Fig.5.

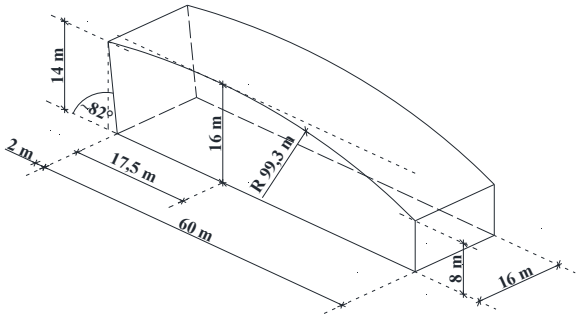

Fig.4. Draft and basic dimensions of the analyzed object body.

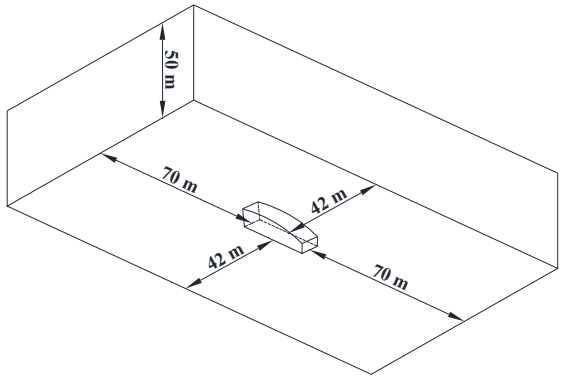

Fig.5. Adopted dimensions of the computational domain.

We have defined five different wind load cases to represent the most dangerous wind pressure fields acting on our structure (Fig.6). The air is modeled here as an incompressible, viscous fluid, whereas the boundary conditions for the wind velocity are assumed by the given constant velocity on the surface closer to the higher (skew) wall of the building and by zero gradients for all fluid flow parameters in the direction normal to the surface on the opposite plane. The "wall" condition, applied to the object surface and to the domain base, assumed neutralization of all velocity components; such an element becomes an obstacle for moving air particles. The domain sides are so distant from the model external vertical boundaries that the air flow is assumed as non-turbulent: boundary condition "symmetry" has been assigned to the rear and the

upper sides (except for the inflow and outflow ones). This boundary condition assumed zero velocity components normal to the surface of the symmetry; the components along the surface remained unchanged. The computational domain – the space between the building body and domain boundaries and the wall surfaces – has been subjected to numerical discretization using the classical Finite Volume Method. A three-dimensional unstructured grid has been used (Tet/Hybrid – tetrahedral hybrid finite volumes, scale 1:1). By applying local grid creation conditions to the domain sides and the building body, a volumetric grid of pyramids has been generated with the minimum skewness of *0.8* for each pyramid.

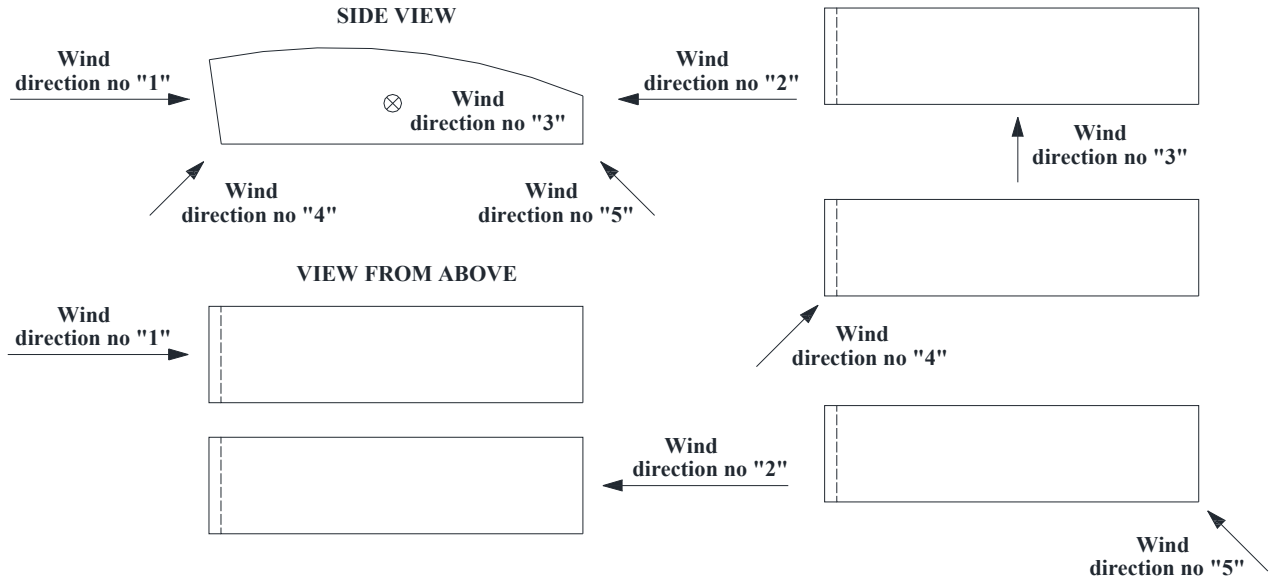

Fig.6. The wind load cases.

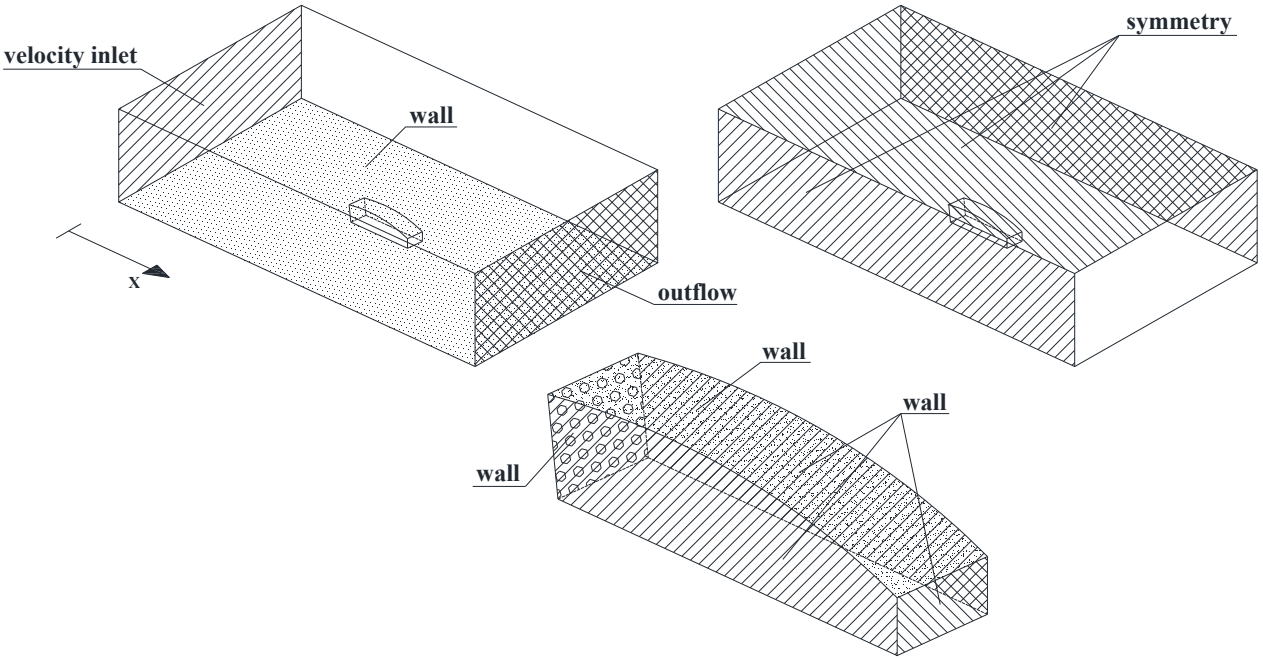

Fig.7. Boundary conditions assigned to given parts of the computational model.

Table 1. Computational domain dimensions and total number of finite volumes.

		Wind direction no "1"	Wind direction no "2"	Wind direction no "3"	Wind direction no "4"	Wind direction no "5"
coordinates	x	*200*	*200*	*170*	*200*	*200*
	y	*100*	*100*	*160*	*100*	*100*
	x	*50*	*50*	*50*	*50*	*50*
Cells		*1071265*	*1069169*	*2311916*	*1069206*	*1068430*
Faces		*2187130*	*2182968*	*4671263*	*2182888*	*2181335*
Nodes		*201315*	*200976*	*409089*	*200899*	*200773*

The exact dimensions of the domain and the number of finite volumes (cells, faces, and nodes) into the computational grid have been presented in Tab.1. The density of the FVM grid has been increased for the regions with larger velocity gradients and decreased, where these gradients were definitely smaller. Our computational grid is set in such a way as to capture all essential flow aspects and to avoid numerical discrepancies like local changes of its density or the cells showing improper distortions. The air flow parameters are set using the wind velocity profile automatically built-in the ANSYS program. This profile includes average wind velocity taking into account terrain roughness, wind direction, and the altitudes. The profile is presented in a graphical form in Figs 8-9. The following parameters for the wind pressure have been adopted: $v_b = 22,0\,\frac{m}{s}$, $c_r(z) = \left(\frac{z}{10}\right)^{0,17}$, $c_o(z) = 1,0$, $v_m(z) = c_r(z) \cdot c_o(z) \cdot v_b$, where z is the altitude.

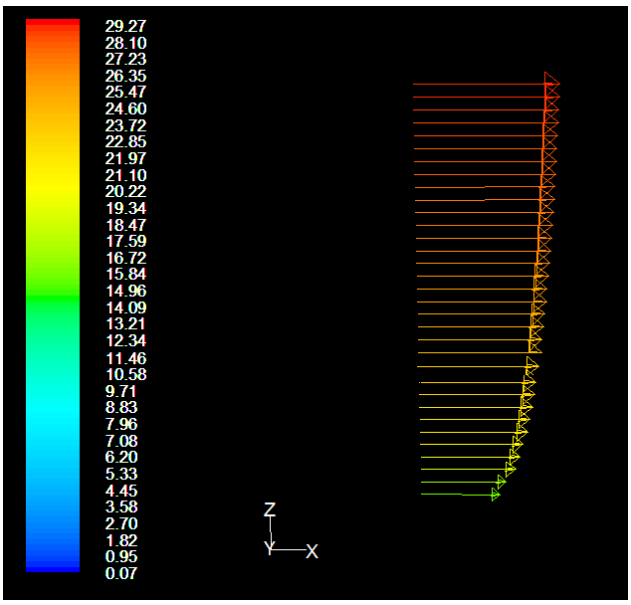

Fig.8. Visualization of the wind velocity profile in the ANSYS 15.0 Fluid Dynamics module.

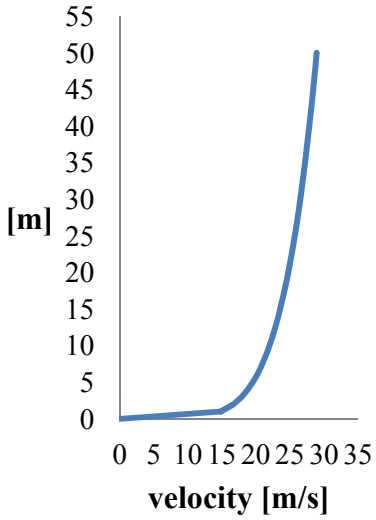

Fig.9. Average wind velocity against the altitude.

5. Discussion of the results

Distribution maps for external pressure coefficients were based on the results of the CFD analysis. Different structure surfaces - the walls and the roof – were divided into some smaller rectangular areas;

vertical walls were divided into several vertical strips, for instance. An orthogonal grid of 7 x 8 areas was chosen for the sloped wall, and an orthogonal grid of 24 x 8 areas, which corresponds to the real layout of structure bars, has been chosen for the roof. The above assumptions were made to allow for the distribution of adequate coefficient values. These grids are subsequently applied to recover the gradual changes of the pressure coefficients.

Having the CFD problem solved we created the maps of coefficients of external pressure for individual parts of the building for any adopted wind direction for the chosen grids. The following rules were applied during this procedure:

- an individual grid cell was assumed to be a surface element, where a single interval of the external pressure coefficient values occurs,
- if one cell had the coefficient value belonging to two different intervals, then more unfavorable values were chosen or the values corresponding to coefficients on a larger surface,
- if coefficients in a given value interval occupied a negligible surface, they were rejected as extreme and unreliable,
- the external pressure coefficient value in a given area was chosen as the least favorable value from its interval.

When the above rules were applied, this problem solution exhibited the occurrence of small values of external pressure coefficients between neighboring grid cells and diligence in preserving its vertical distribution. The results evaluated under the above assumptions are presented for a few exemplary surfaces and wind directions in Figs 10-15.

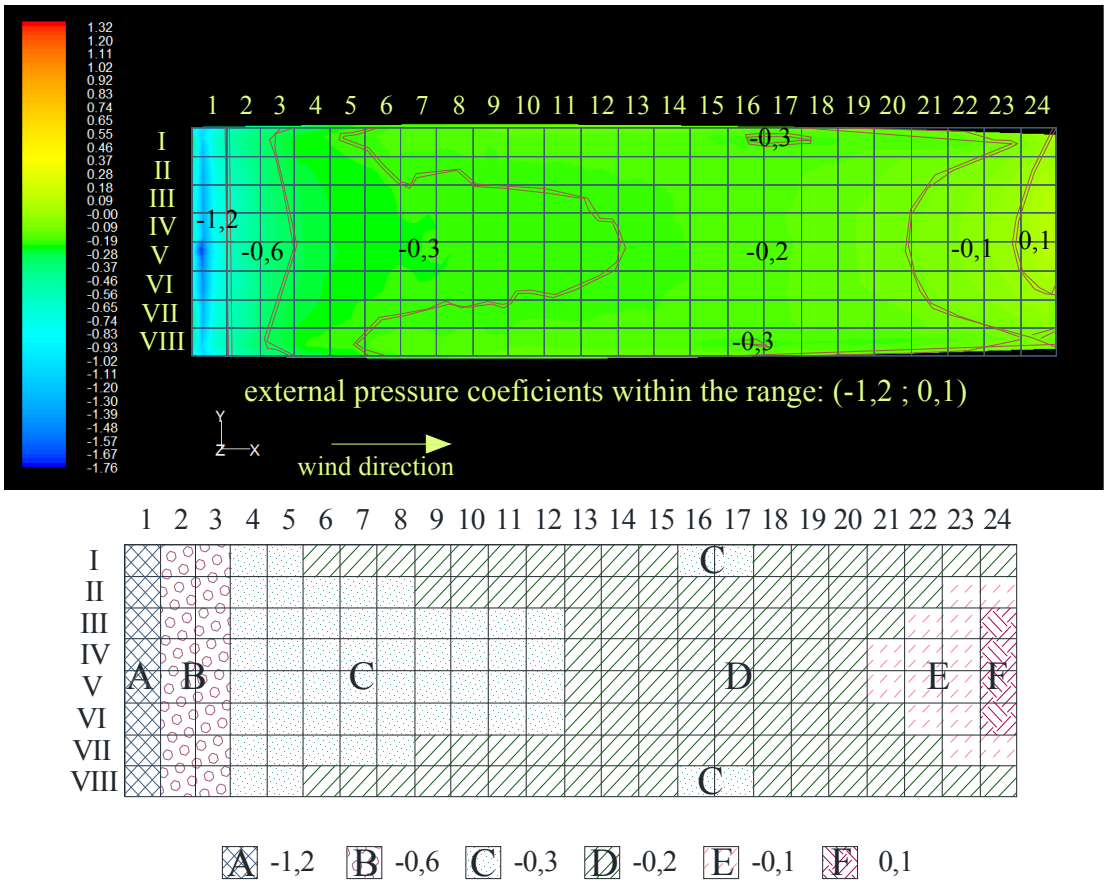

Fig.10. External pressure coefficient maps for the roof surface for wind in direction „1”.

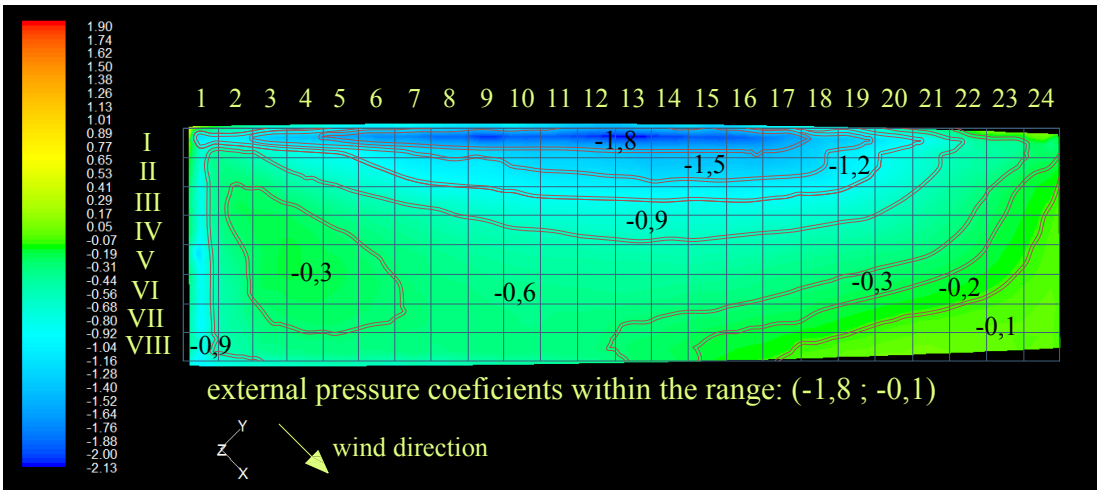

Fig.11. External pressure coefficient maps for the roof surface for wind in direction "4".

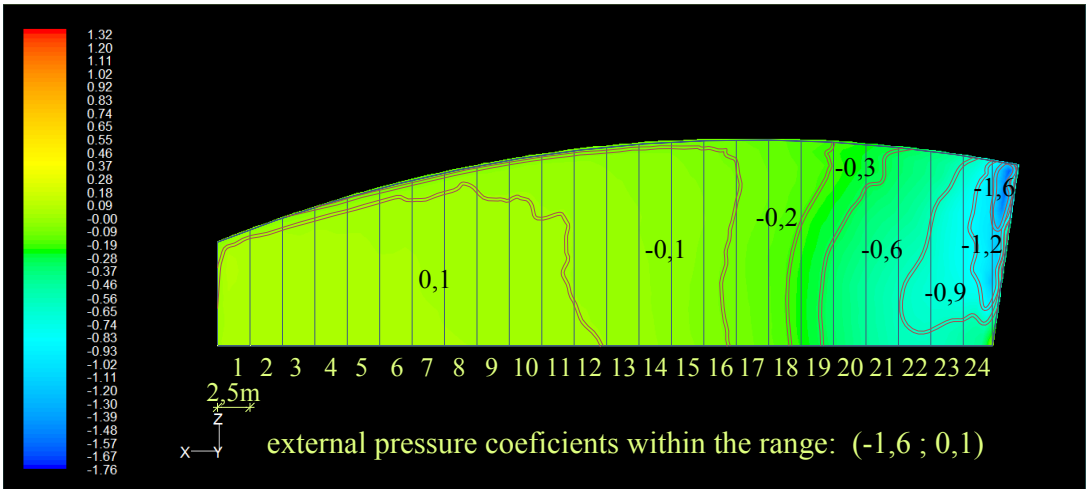

Fig.12. External pressure coefficient maps for the wall surface for wind in direction "1".

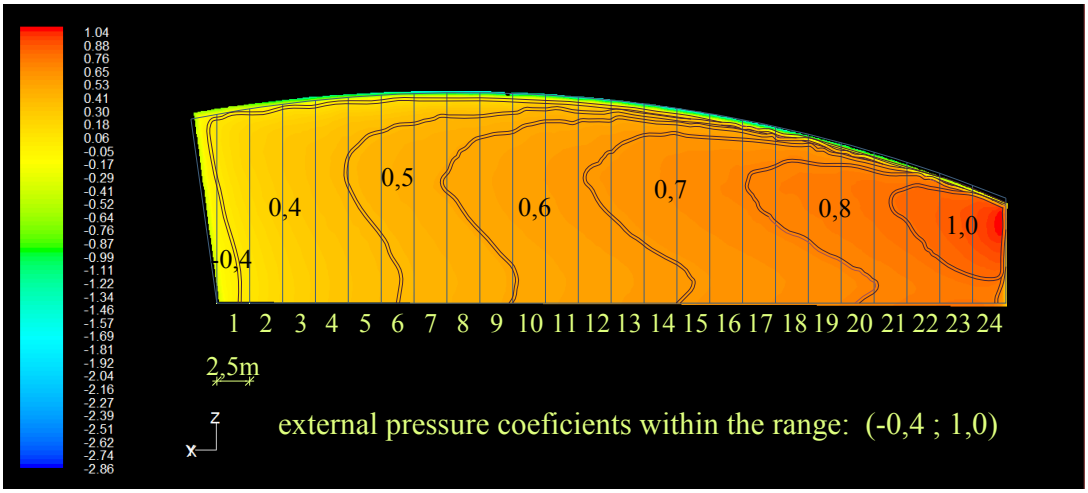

Fig.13. External pressure coefficient maps for the wall surface for the wind in direction "5".

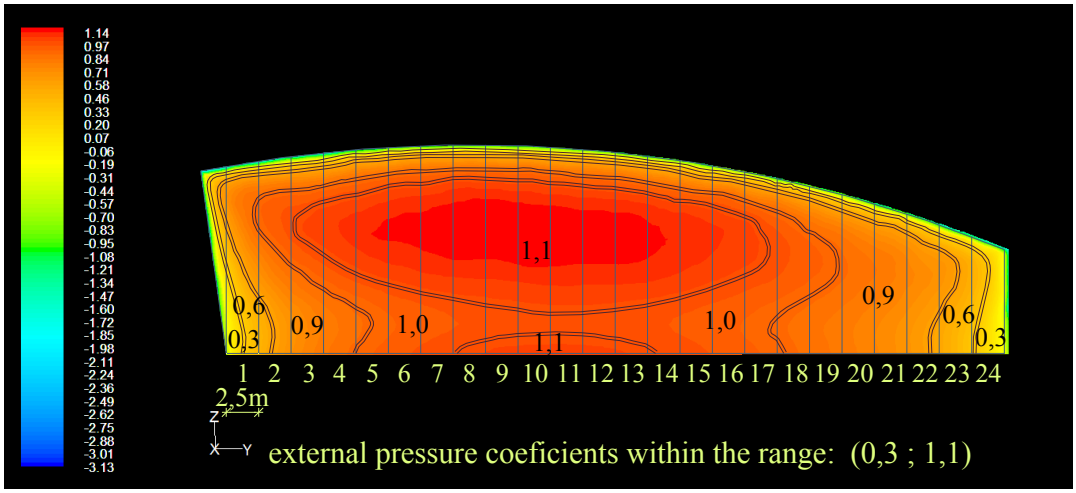

Fig.14. External pressure coefficient maps for the wall surface for the wind in direction "3".

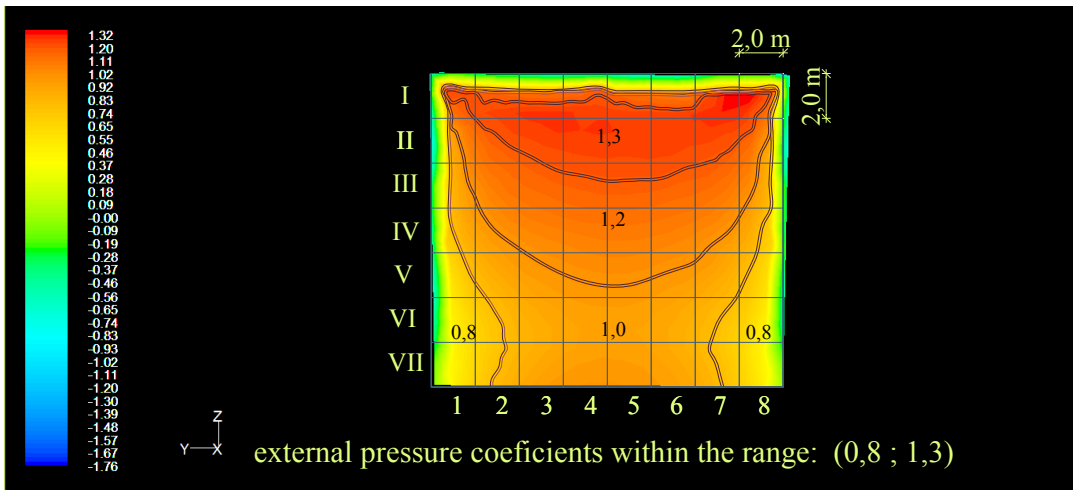

Fig.15. External pressure coefficient maps for the sloped wall surface for the wind in direction "2".

Further, we proceeded with transitions of the data from the CFD analysis of the obtained results into the structural model; the linearization of the results and the division of the surface into individual areas allows a direct transfer of the CFD analysis results into the FEM structural model (Fig.16).

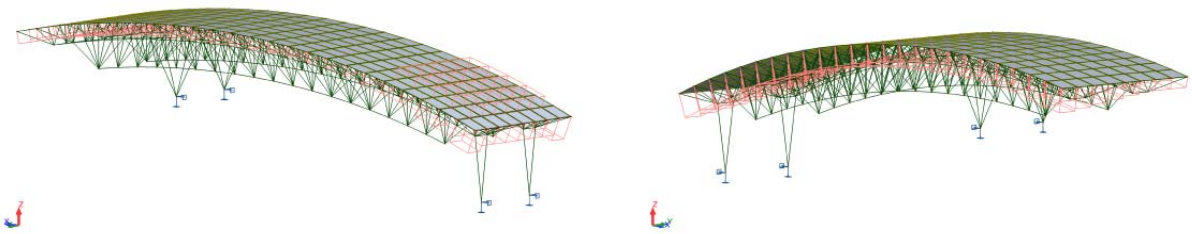

Fig.16. Results of the CFD analysis: wind blows in directions 2 (left) and 3 (right).

The Finite Element Method model of the representative structural element was prepared with the use of 359 nodes, 1158 two-noded 3D beam elements and 192 non-material surface elements, where an external load was applied. The load condition of the object included deadweight, snow action estimated based on standard [31] and wind action as leading variable actions. All these environmental loads were combined according to the scheme provided by [32]. The distributions of the internal forces, which include axial forces and bending moments in individual structural members, are shown below.

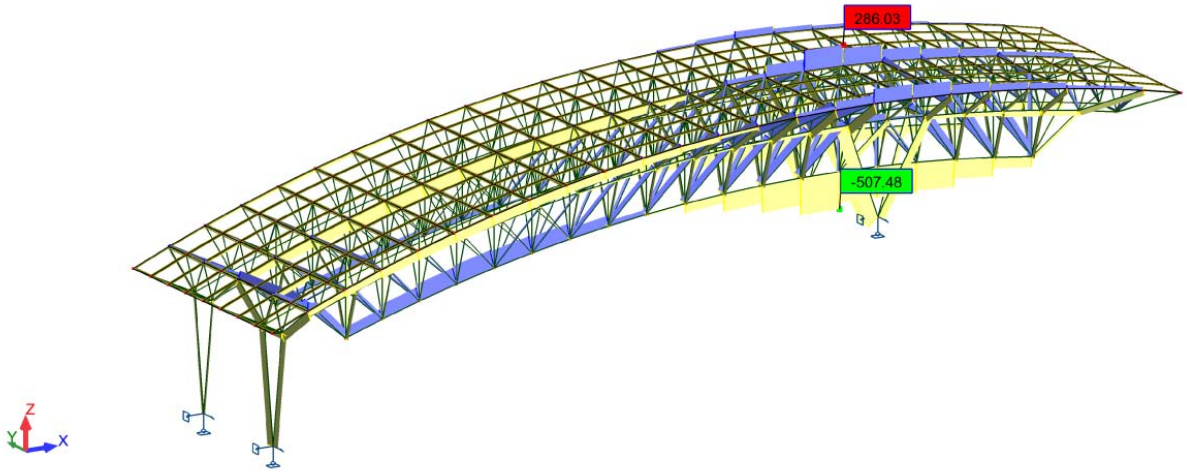

Fig.17. Axial forces in particular structure members.

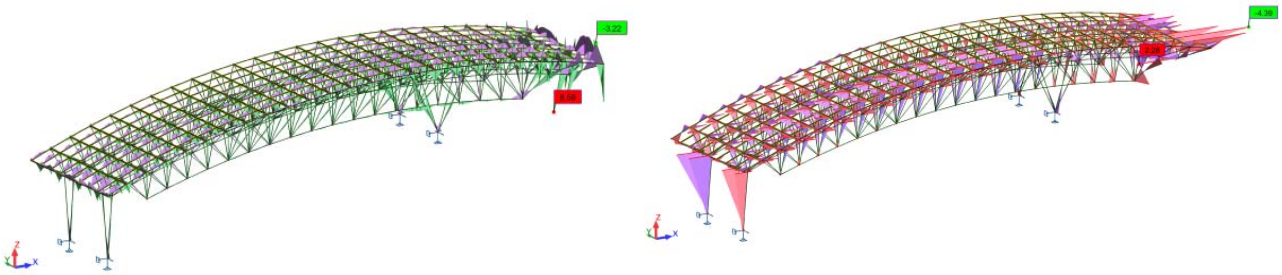

Fig.18. Bending moments diagrams M_y (left) and M_z (right) in structural members.

The above results show that extreme values of the axial forces occurred around bearing elements: poles at the level above the structure depicted in Fig.17. Maximum compression forces occurred in the first layer of arcs and maximum tensile forces in the third one. Maximum bending moments occurred around the roof edge, the one located higher (Fig.18).

A substantial aspect that deserves a separate discussion is the structural displacements diagram. Figure 19 presents global displacements of these nodes in the Serviceability Limit State (SLS).

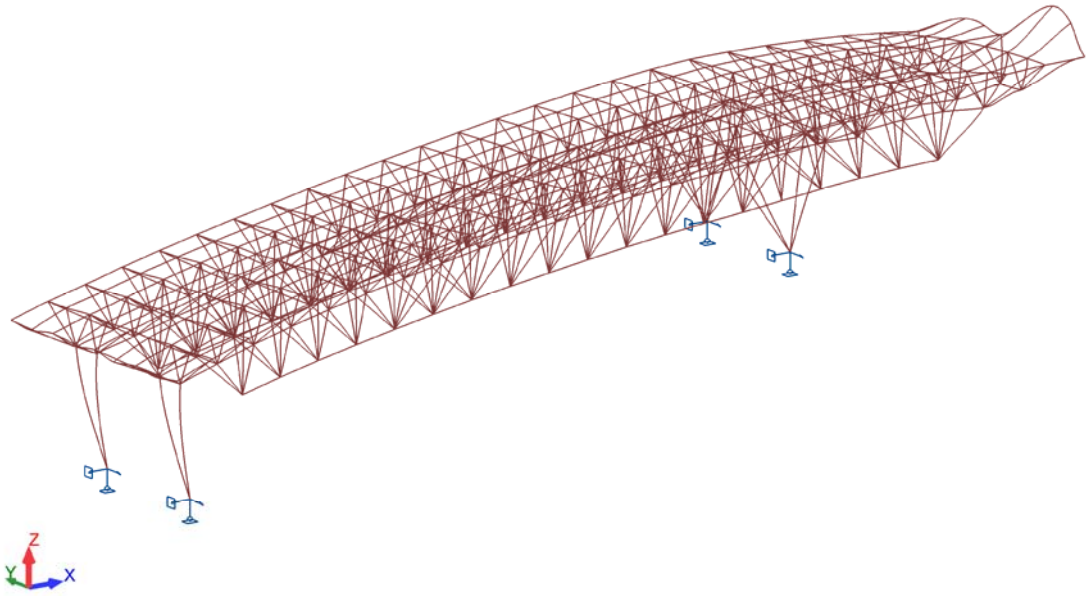

Fig.19. Displacements of the representative structural spatial element.

Maximum deformations occurred at the higher roof edge, where the wind suction has an extreme value. The gravity load, although acting in the opposite direction than for the structural model (layout of bearing elements and loads), affected the object negatively and increased the deformation of the structure. Based on the static strength analysis it can be stated that the elements under the largest stresses are close to the supporting bearing elements as well as the cover elements, where the maximum strain occurred due to the wind action. The degrees of structural effort for particular element groups are presented in Tab.2.

Table 2. Effort level in the specific structural elements groups.

Groups of the structural members	**Effort degree**
Terminal and middle arcs of the first layer	*89.1 %*
Other arcs and transverse elements of the first layer	*85.3 %*
Elements of the second layer	*88.0 %*
Elements of the third layer	*89.2 %*
Elements of the vertical walls	*88.3 %*
Bracing elements	*88.9 %*
Pole rebars of lower level	*83.0 %*
Pole rebars of higher level	*86.0 %*

The maps of external pressure coefficients, velocity vectors along the walls, and streamlines (the lines of field of velocity vectors parallel to a given velocity vector at a given point) are presented all in Figs

20-25. They approximately represent the wind flow around the building. After analyzing the coefficient maps for the walls of the structure, we can notice that the wind suction was dominating for the walls that are parallel and leeward to the wind flow direction, wherein the more distant from the windward wall, the higher the values of pressure coefficients; they fluctuate from negative to positive values. A more remarkable wind influence can be observed on vertical edges for the leeward wall. The maximum values of pressure coefficients can be found in the central areas for the surfaces pressed by the wind (at about 2/3 of the wall height); the pressure systematically decreases there while approaching the edges.

Although the wind flow as a turbulent flow was chaotic, some regularity could be noticed during an observation of the mentioned wind behavior parameters. When an air stream encountered an obstacle, such as a building, it stopped at about 2/3 of its height exhibiting a characteristic stagnation point, which is remarkable in Figs 20-21 containing velocity vectors and streamlines around the structure.

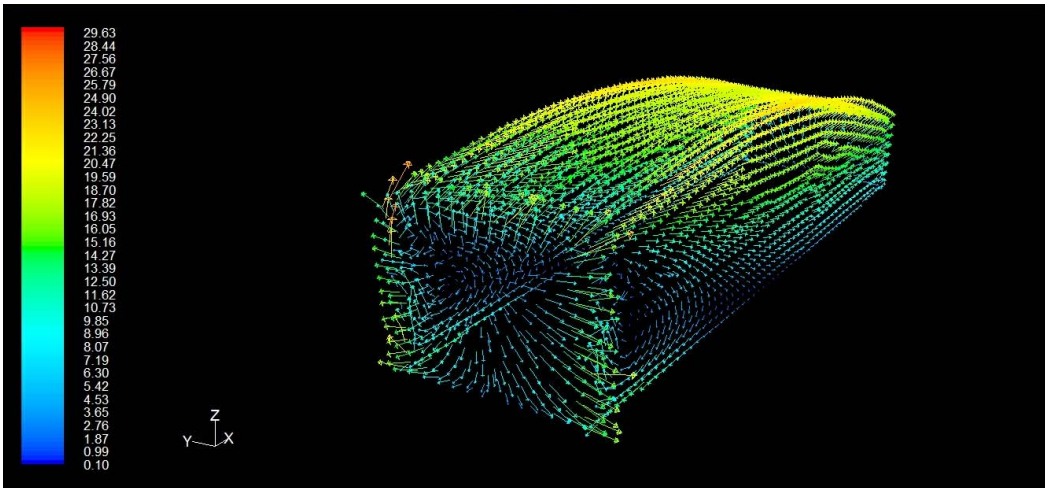

Fig.20. Velocity vectors around the analyzed object for the wind in direction "1".

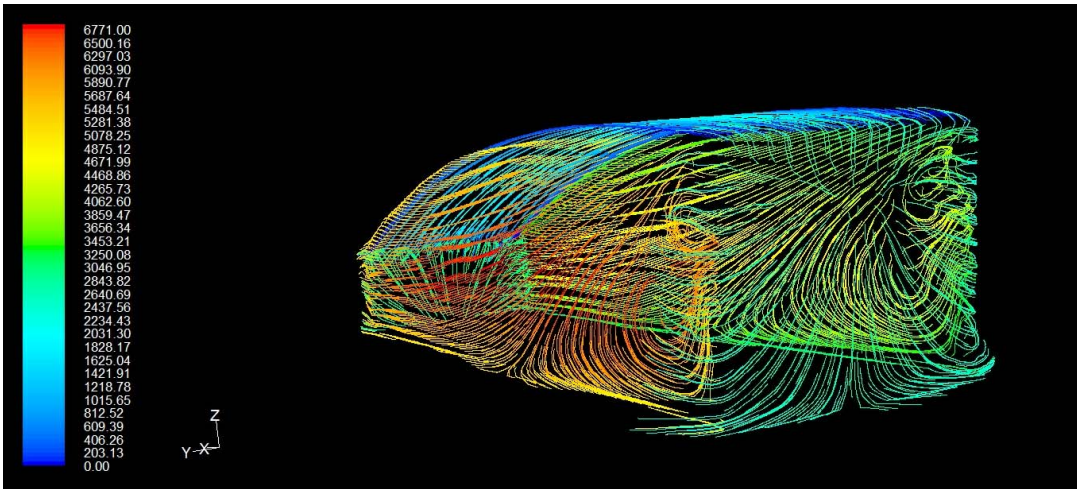

Fig.21. Streamlines around the analyzed object for the wind in direction "1".

Below that point the air ”flows off” down on a building wall creating a frontal vortex at the contact with the ground. The rest of the air flows around the walls and the roof. The behavior at the windward wall edges, where the separation of air streams occurs (Figs 22-23), also needs to be outlined.

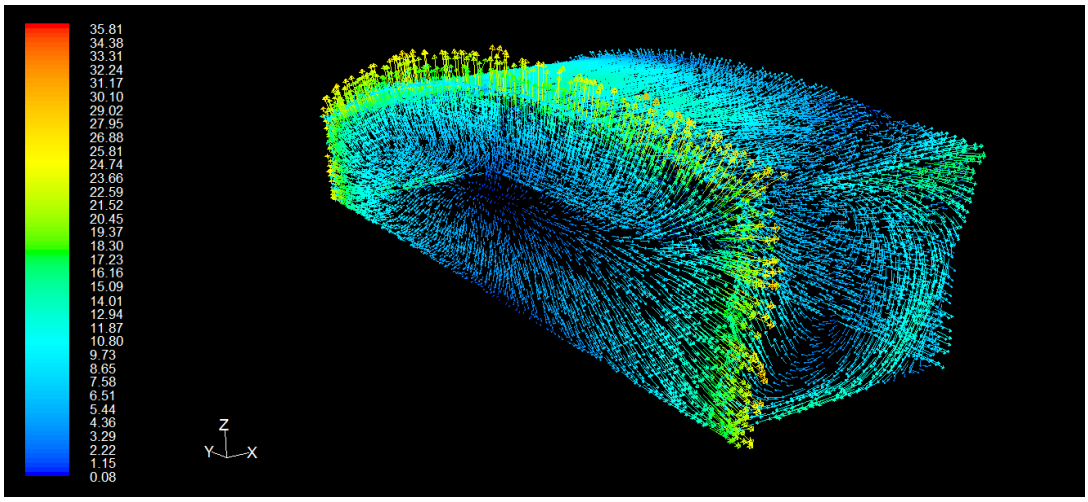

Fig.22. Velocity vectors around the analyzed object for the wind in direction "3".

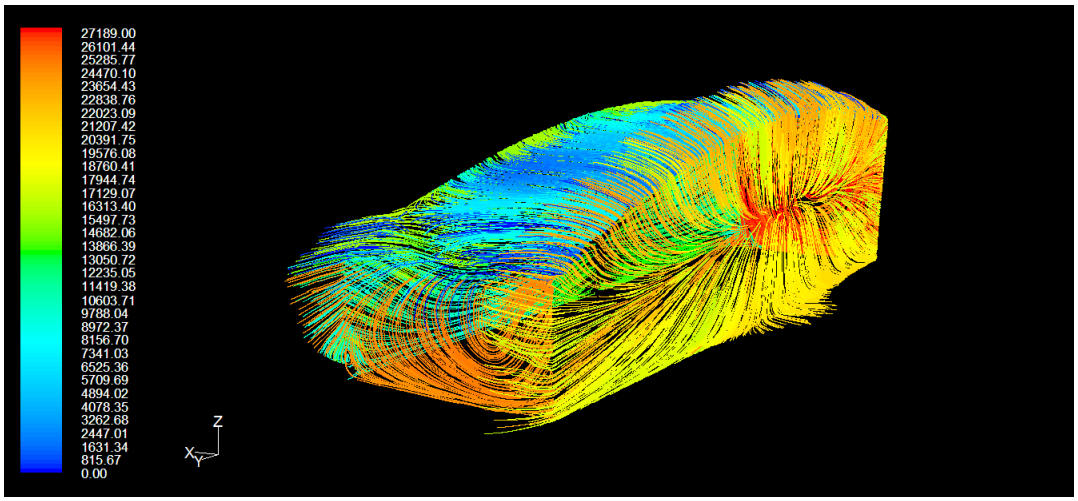

Fig.23. Streamlines around the analyzed object for the wind in direction "3".

The air velocity increased significantly at the windward wall edges and a negative pressure region appeared, which is clearly visible in external pressure coefficient maps generated by the CFD software (Figs 13-15). If the wind presses a wall, it is obvious that the external pressure coefficients adopt positive values. The negative values of coefficients could be found at the edges of the wall. Their values were often comparable to or even greater than the coefficient values corresponding to pressing. Still, the surfaces where the separation of air streams occurs were negligibly small compared to positive pressure surfaces; therefore such a suction was omitted in the calculation of the wind load.

The air that flowed around the lateral walls exhibiting negative pressure, further flowed down towards the base of the building and created vertical vortices that underwent acceleration generating strong airstreams at the corners, which is depicted in Fig.24.

After flowing around the obstacle, a part of the momentum was lost and an area of weakened flow was created behind the building. The air flowing over the building was divided at the back into two parts, one of which recirculated (recirculation area), and the other flowed by (far-wake area). The vertical vertices were created at the edges of the leeward wall.

The flow scheme depicted above for the flow around the building is noticeable particularly for the wind in directions “2” and “3”; the model and external pressure coefficient distribution differ accordingly for

a skewed flow. In addition, it can be noticed that, although the distribution of coefficients on vertical walls creates approximately vertical stripes (used for the division into areas in [29]), such a division was not made in the case of a sloped wall, where the distribution adopted totally different characteristics that were more similar to a division into horizontal areas, which is an approximation as well. In that case, it is justified to use a standard approach for vertical walls of the structure only; adopting the same assumptions for sloped walls would result in errors in spite of the fact that the slope was only about 8 degrees in relation to the vertical line.

All external pressure coefficients, velocity vectors, and streamlines excellently depict characteristic vortex structures for the fluid flow. The velocity vectors distribution and streamlines on the surface of the analyzed object for individual wind load cases are presented below.

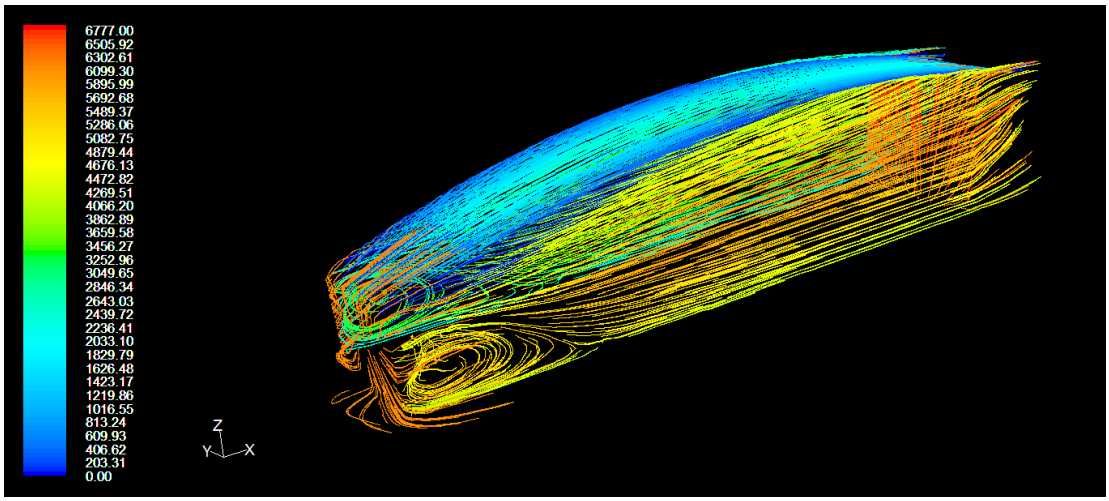

Fig.24. Streamlines around the analyzed object for the wind in direction „2”.

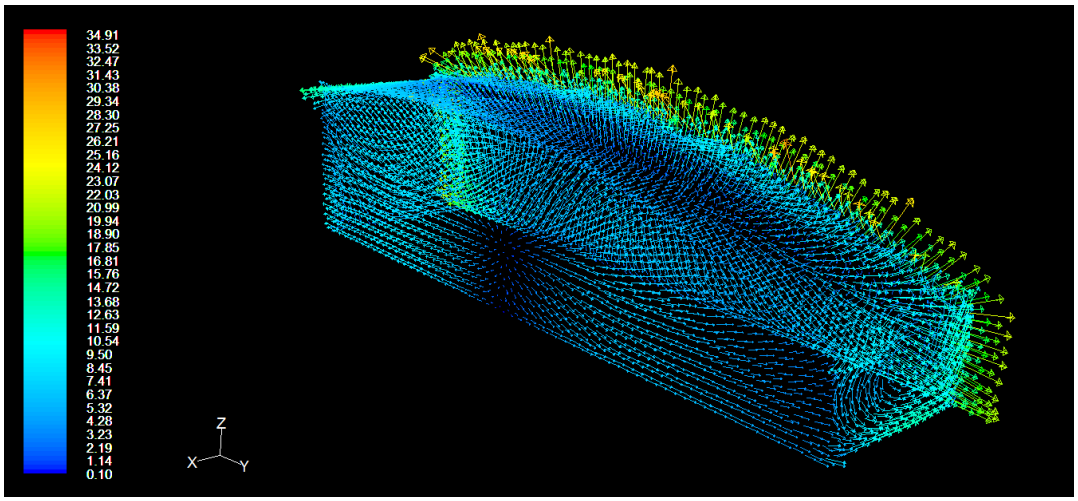

Fig.25. Velocity vectors for the wind in direction „3”.

6. Conclusions

The aim of this work was to perform a CFD analysis for the wind flow around a building of a non-standard body and a precise determination of the influence of the wind load on individual surfaces of the structure. It is particularly important in the design of structural grid roof covers, where precise estimation of

internal forces determines if the project realization is feasible and optimal. All external pressure coefficients acting on the walls and on the roof as well as the velocity vectors and streamlines around the walls and roof shell of the analyzed structure have been determined. The major conclusions which can be drawn from this analysis may be formulated as follows:

- the results indicate that it is possible to find the precise external pressure coefficients distribution for individual surfaces of a given structure,
- the external pressure coefficient maps, which have been created, can be successfully used as a basis for a relatively precise determination of the wind load for this structure; and what is even more important, they can be also directly implemented into the FEM model using a variety of the available commercial and academic software,
- the external pressure distribution within the structure wall sloped 82 degrees in relation to the terrain level appears to be remarkably different compared to other vertical walls; it seems that very frequently the assumption that almost vertical walls may be treated in a standard way (as vertical walls) may lead to a remarkable modeling error,
- CFD analysis coupled with the FEM models constitutes a useful tool in the design process allowing the computation of relatively realistic wind load on solids and surfaces of quite non-standard dimensions as well as a proper determination of the effort level of the structural members.

The proposed computational approach offers an efficient support in wind load estimation and modeling for structures being designed, especially when they are particularly sensitive to this load. The large scale structures such as long-span roofs seem to require special designing attention and effort, where analysis data can make a remarkable difference between project success and failure. It needs to be mentioned that the successfully coupled implementation of the FVM and FEM may be very beneficial in further stochastic models of the wind blow and its impact on engineering structures, that can result in stochastic both time-independent and dependent reliability assessments, cf. [11]. Such an advantageous approach may include stochastic variations in both wind direction and speed, some material uncertainties and geometrical imperfections inside the structure as well as especially interesting and challenging stochastic waviness in the object external walls affecting both – the combined FVM-FEM solution as well as its stochastic counterpart.
The proposed interfacing procedure in-between the FVM and the FEM computer programs is not very efficient, because it does not allow directly incremental nonlinear problems solution where solid body deformations affect initial distribution of the wind pressures and velocities and vice versa, contrary to the well-known BEM-FEM programs, c.f. [33], where two methods may be incorporated into the single computer code. Full interfacing would demand the same density of the grid (in the FVM) and the mesh (in the FEM) close to the fluid-structure interface as well as connection of the nodes in the grid (lying in the middle of the outer finite volume surfaces) with the nodes in the mesh (the ends of 3D beam finite elements or at the ends of 4-noded shell elements).

Nomenclature

A_j – area of the j face
$B_{ij\alpha}(x)$ – matrix of the shape functions derivatives
$C_{\varepsilon 1}$, η, s, s_{ij}, G_k, μ_l – parameters of k-ε model
$C_{ijkl}^{(e)}$ – elasticity tensor components inside the finite element e
$c_r(z)$ – roughness factor
$c_o(z)$ – orography factor
E – total number of finite elements within Ω
e – number of finite element
f_i – vector component of body forces

$\overline{f_i}$ – average value of external forces vector component (unit mass forces)
g – gravitational acceleration
i, j – Cartesian coordinates in three dimensional flow
$K_{\alpha\beta}$ – stiffness matrix
k – turbulence kinetic wind energy
l – number of finite volume
M – total number of computational iterations
N – total number of degrees of freedom introduced in Ω
n_j – surface A_j versor directed outwards
p – static pressure
$\overline{p}$ – average value of static pressure
t – time
Q_d – external forces vector
q_β – resulting displacement vector
V_l – the lth finite volume
v_b – basic wind velocity
v_i – velocity vector component
$\overline{v}_i$ – average value of velocity vector component
z – altitude
$\nabla P_l^{(\alpha)}$ – pressure gradient
Δt – time increment
δ_{ij} – Kronecker delta
ε – turbulence dissipation coefficient
ε_{ij} – small strain tensor
μ – dynamic viscosity coefficient
μ – fluid viscosity
ν – kinematic viscosity coefficient
$v_m(z)$ – mean wind velocity
ρ – density of the medium
$\overline{\tau}_{ij}$ – turbulent stresses
$\phi_{i\alpha}(x)$ – classical shape function
Ω – computational domain
∇^2 – Laplace operator
$\partial\Omega_\sigma$, $\partial\Omega_u$ – external boundaries of Ω

References

[1] Editorial (2013): *CFD simulation of pedestrian-level wind conditions around buildings: Past achievements and prospects*. – Journal of Wind Engineering and Industrial Aerodynamics, vol.121, pp.138-145.

[2] Mak C.M., Niu J.L., Lee C.T. and Chan K.F. (2007): *A numerical simulation of wing walls using computational fluid dynamics.* – Energy and Buildings, vol.39, pp.995-1002.

[3] Blocken B. and Carmeliet J. (2007): *Validation of CFD simulations of wind-driven rain on a low rise building façade*. – Building and Environment, vol.42, pp.2530-2548.

[4] Chavez M., Hajra B., Stathopoulos T. and Bahloul A. (2011): *Near field pollutant dispersion in the built environment by CFD and wind tunnel simulations*. – Journal of Wind Engineering and Industrial Aerodynamics, vol.99, pp.330-339.

[5] Huang S. et al. (2007): *Numerical evaluation of wind effects on a tall steel building by the CFD.* – Journal of Constructional Steel Research, vol.63, pp.612-627.

[6] Menter F.R. (2011*): Turbulence modeling for engineering flows*. – A Technical Paper from ANSYS. - Inc, pp.1-25.

[7] Chung T.J. (2010): *Computational Fluid Dynamics.* – Cambridge University Press.

[8] Ferziger J.H. and Perić M. (2002): *Computational Methods for Fluid Dynamics*. – Germany: Springer-Verlag, Berlin-Heidelberg.

[9] Flaga A. (2008): *Wind Engineering. Fundamentals and Applications* (in Polish). – Warsaw, Poland: Arkady.

[10] Vizotto I. and Ferreira A.M. (2015): *Wind force coefficients on hexagonal free form shell.* – Engineering Structures, vol.83, pp.17-29.

[11] Kamiński M. (2013): *The Stochastic Perturbation Methods for Computational Mechanics*. – Chichester: Wiley.

[12] Zhang Y., Habashi W.G. and Khurram R.A. (2015): *Predicting wind - induced vibrations of high-rise buildings using unsteady CFD and modal analysis.* – Journal of Wind Engineering and Industrial Aerodynamics, vol.136, pp.165-179.

[13] Hoof van T., M. Blocken and Harten van M. (2011): *3D CFD simulation of wind flow and wind-driven rain shelter in sports stadia: Influence of stadium geometry.* – Building and Environment, vol.46, pp.22-37.

[14] Blocken B. and Persoon J. (2009): *Pedestrian wind comfort around a large football stadium in an urban environment: CFD simulation, validation and application of the new Dutch wind nuisance standard*. – Journal of Wind Engineering and Industrial Aerodynamics, vol.97, pp.255-270.

[15] Blocken B., Janssen W.D. and Hoof van T. (2012): *CFD simulation for pedestrian wind comfort and wind safety in urban areas: General decision framework and case study for the Eindhoven University campus*. – Environmental Modelling & Software, vol.30, pp.15-34.

[16] Oggiano L. (2014): *CFD simulations of the NTNU wind turbine rotor and comparison with experiments*. – Renewable Energy Research Conference*,* vol.58, pp.111-116.

[17] Li Y., Castro A., Sinokrot T., Prescott W. and Carrica P. (2015): *Coupled multi-body dynamics and CFD for wind turbine simulation including explicit wind turbulence*. – Renewable Energy, vol.76, pp.338-361.

[18] Tominaga Y., Shin-ichi Akabayashi, Takuya Kitahara and Yuki Arinami (2015): *Air flow around isolated gable-roof buildings with different roof pitches: Wind tunnel experiments and CFD simulations.* – Building and Environment, vol.84, pp.204-213.

[19] Montazeri H. and Blocken B. (2013): *CFD simulation of wind-induced pressure coefficients on buildings with and without balconies: Validation and sensitivity analysis.* – Building and Environment, vol.60, pp.137-149.

[20] Kamiński, M. and Ossowski, R. L. (2009): *The Stochastic perturbation – based Finite Volume Method for the flow problems.* – Journal of Technical Physics, vol.50, No.1, pp.297-315.

[21] Kamiński M. (2001): *Stochastic problem of viscous incompressible fluid flow with heat transfer.* – Zeitschrift für Angewandte Mathematik und Mechanik, vol.81, No.12, pp.827-837.

[22] Cueto – Felgueroso L. and Peraire J. (2008): *A time - adaptive Finite Volume Method for the Cahn-Hilliard and Kuramoto – Sivashinsky equations*. – Journal of Computational Physics, vol.227, pp.9985-10017.

[23] Durany J., Pereira J. and Varas F. (2006): *A cell-vertex finite volume method for thermo-hydrodynamic problems in lubrication theory.* – Computer Methods in Applied Mechanics and Engineering, vol.195, pp.5949-5961.

[24] Fallah, N. (2004): *A cell vertex and cell-centered finite volume method for plate bending analysis.* – Computer Methods in Applied Mechanics and Engineering, vol.193, pp.3457-3470.

[25] Kamiński M. and Carey G.F. (2005): *Stochastic perturbation-based finite element approach to fluid flow problems.* – International Journal of Numerical Methods in Heat and Fluid Flow*,* vol.15, No.7, pp.671-697.

[26] Kamiński M. and Ossowski R.L. (2009): *The Stochastic perturbation – based Finite Volume Method for the flow problems.* – Journal of Technical Physics, vol.50, No.1, pp.297-315.

[27] Stacharska–Targosz J. and Chmielowiec M. (2008): *Application of finite volume method for numerical calculations of the cross flow fan performance curves*. – Archives of Thermodynamics, vol.29, No.2, pp.3-20.

[28] Zienkiewicz O.C. and Taylor R.L. (2005): *The Finite Element Method for Fluid Dynamics*. – Amsterdam: Elsevier.

[29] Eurocode 1 (2008): *Actions on structures, Part 1-4: General actions - Wind actions*. – Warsaw.

[30] Franke, J. (edr.) (2004): *Recommendations on the Use of CFD in Wind Engineering*. – Brussels.

[31] Eurocode 1 (2005): *Actions on structures*, *Part 1-3: General actions - Snow actions*. – Warsaw.

[32] Eurocode 0 (2004): *Basis of structural design*. – Warsaw.

[33] Wolf J.P. (2003): *The Scaled Boundary Finite Element Method*. – Chichester: Wiley.

Received: January 31, 2017

Revised: September 8, 2017